Reconfigurable Liquid Metal Based SIW Phase Shifter

Shaker Alkaraki, *Member, IEEE,* Alejandro L. Borja, *Member, IEEE,* James R. Kelly, *Member, IEEE,*
Raj Mittra *, Life Fellow, IEEE,* Yue Gao*, Senior Member, IEEE*

Abstract—**This paper presents the first substrate integrated waveguide (SIW) phase shifter that can be reconfigured using liquid metal. This digital phase shifter exhibits low insertion loss and is reciprocal and bidirectional. It incorporates a series of holes which can be filled or emptied of liquid metal, enabling us to add or remove via connections dynamically, on-the-fly. By using a collection of such holes, it is possible to create a wall along the E-plane or H-plane of the waveguide. When the wall is in place, it blocks the passage of energy. When the wall is absent, energy is able to flow. In this way, it is possible to guide the electromagnetic (EM) waves through 1 of 3 paths, having different electrical lengths. The result is a digital switched-line phase shifter that achieves coarse steps of phase change, from 0° up to 180°, in steps of 60°. By filling or emptying individual holes it is possible to introduce reactive loading into each path. In this way it is possible to achieve fine phase control in steps of 10°. By employing both forms of reconfiguration in unison the proposed phase shifter is able to deliver a phase shift of up to 180°, in steps of 10°. The proposed phase shifter operates at 10 GHz and exhibits an insertion loss of less than 2.3 dB over its entire operating band. Furthermore, the underlying concept of the proposed phase shifter can be readily scaled for operation in the millimeter wave band. Existing phase shifters operating in that band exhibit significant insertion losses. Millimeter wave phase shifters are expected to find application in 5G mobile access points.**

Index Terms—**Liquid metal, reconfigurable phase shifter, SIW.**

I. INTRODUCTION

PHASE shifters are essential components of several microwave and millimeter-wave (mm-wave) systems, such as: phased arrays, smart antennas, modulators and microwave instrumentation. However, the majority of passive phase shifters suffer from high insertion loss at microwave and mm-wave frequencies. For example, the average insertion loss of a phase shifter, operating at X-band frequencies (i.e. 10 GHz), is 4.69 dB (with a variance of 5.24 dB) [1]-[20]. The insertion loss can be mitigated by employing active phase shifters, which incorporate integrated amplifiers. However, active phase shifters consume considerably more DC power than passive ones. For this reason, one could argue that active phase shifters are ill-suited for power-constrained applications.

Of the X-band phase shifters, reported in the literature, it is those employing mechanical reconfiguration or MEMS-switched capacitors that offer the lowest insertion losses. However, the use of mechanical moving parts increases the need for maintenance and repair. On the other hand, MEMS suffer from a range of disadvantages, including poor reliability, e.g. due to contact welding, which has prevented their widespread use.

Liquid metals, based on alloys of Gallium, have already been used to design several reconfigurable microwave devices, e.g., filters [21]-[25], switches [26]-[28] and antennas [29]-[32]. One paper presents a phase shifter that can be reconfigured using liquid metal [33]. The design was based around a defected ground plane. The phase shifter operated at 5.6 GHz and provided a total phase shifting range of 67.2° in uneven steps. For the first time this paper proposes a substrate integrated waveguide (SIW) phase shifter that can be reconfigured by using liquid metal technology. The phase shifter exhibits low insertion loss. The phase state is altered by filling and emptying vias with liquid metal. The performance of the proposed phase shifter has been validated numerically and experimentally. Relative to competing devices, the proposed phase shifter is expected to offer significantly improved linearity [29]. Despite slower reconfiguration time (expected to range from seconds to milliseconds [12], [34]) the proposed phase shifter is suitable for applications for which high power-handling capability and low loss are priorities.

The remainder of the paper is organized as follows. Section II discusses the concept and structure of the proposed phase shifter. Section III explains the design process. Section IV discusses fabrication considerations. Section V presents results.

Shaker Alkaraki and James Kelly are with The Antennas & Electromagnetics Research Group, which is based in The School of Electronic Engineering and Computer Science, Queen Mary University of London, Mile End Road, London (email: s.m.alkaraki@qmul.ac.uk; shaker.alkaraki@ieee.org; j.kelly@qmul.ac.uk).

Alejandro L. Borja is with the Departamento de Ingeniería eléctrica, electrónica, automática y comunicaciones, Escuela de Ingenieros Industriales de Albacete, Universidad de Castilla-La Mancha, Campus Universitario, 02071 Albacete, Spain (e-mail: alejandro.lucas@uclm.es).

Raj Mittra is with the Electrical and Computer Engineering Department of the University of Central Florida (UCF) in Orlando, FL, USA. and also with the King Abdulaziz University, Jeddah 21589, Saudi Arabia (e-mail: rajmittra@ieee.org).

Yue Gao is with the ICS, Home of the 6GIC, University of Surrey, UK (email: yue.gao@surrey.ac.uk).
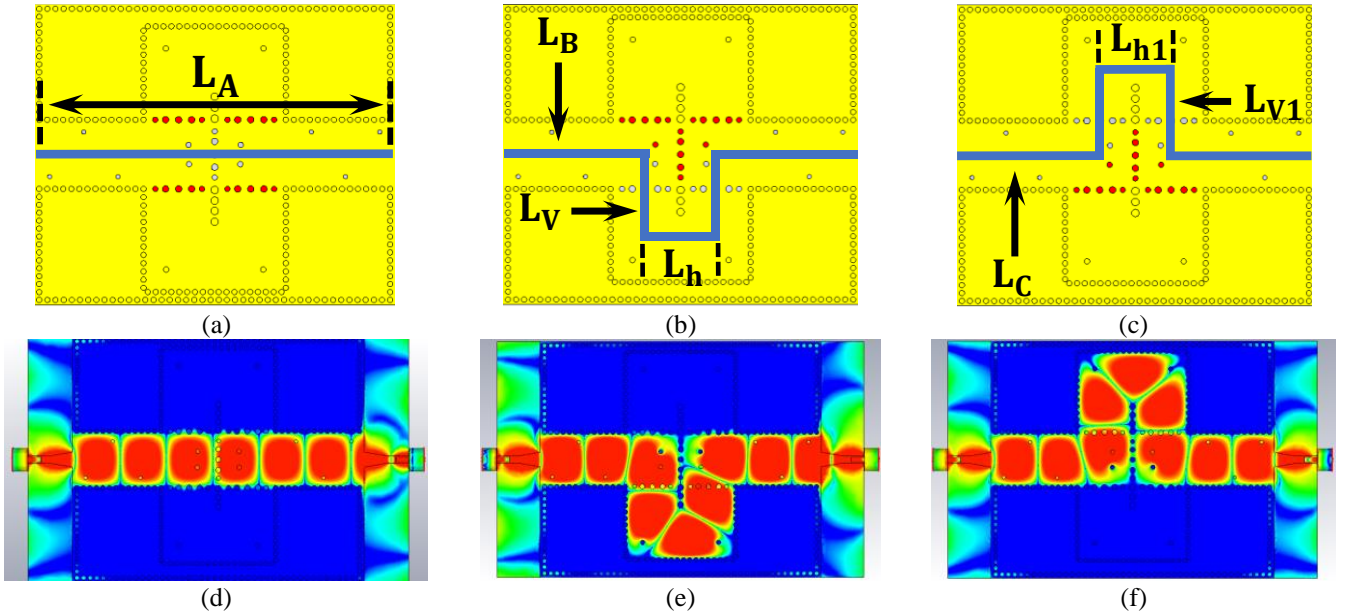
Fig. 1. (a) to (c) Schematics illustrating the 3 main operating states of the proposed phase shifter, namely (a) state A = - 60°, (b) state B = - 120°, and (c) state C = - 180°. (d) to (f) The electric field (E-field) distributions corresponding to states A to C, respectively.

Finally, Section VI, draws conclusions.

II. CONCEPT AND STRUCTURE OF THE SIW PHASE SHIFTER

The proposed phase shifter is based on SIW technology. SIW technology combines some of the advantages of conventional hollow waveguide, such as low loss and high power-handling capability, together with advantages of planar technology such as ease of fabrication. Fig. 1 illustrates the operating principle behind the switched-line aspect of the proposed phase shifter. Fig. 2 indicates the important the dimensions of the proposed phase shifter. Table I gives the numerical values of those dimensions. The proposed phase shifter employs two different stages of reconfigurable phase shift in concert, in order to achieve fine-grained phase control over a 180° phase-shifting range. Specifically, the concept relies on achieving coarse changes in phase shift, by means of a switched-line phase shifter, alongside fine changes in phase shift, by means of reactive loading. By combining these two different forms of reconfiguration, the proposed phase shifter is able to achieve a phase shifting range of 0° to 180°, in steps of 10°.

A. Switched-Line SIW Phase Shifter for Coarse Phase Steps

In the proposed phase shifter, coarse changes in phase shift are realized by guiding the travelling electromagnetic (EM) waves through paths that have different electrical lengths. Reconfiguration between these different paths is achieved by using switches formed from liquid metal. Each switch consists of a group of holes drilled into the substrate. When a particular set of holes are filled with liquid metal, a blocking wall is formed which prevents the propagation of traveling electromagnetic waves. Blocking walls can be added along either the E-plane or H-plane of the waveguide. In this way, the blocking walls are used to reconfigure between three operating states which correspond to paths having different electrical lengths, namely: state A: −60°; state B: −120°; and state C: −180°.
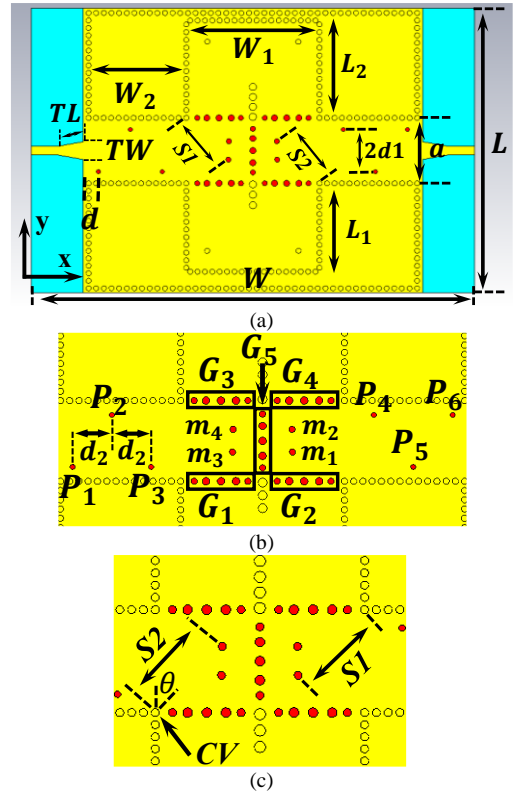

(a)

(b)

(c)

Fig. 2. The schematic of the proposed phase shifter. (a) Top view showing the dimensional parameters, and (b-c) Top view incorporating labels for the walls and vias. Key: substrate = blue, copper = yellow, copper plated vias = yellow, liquid metal vias = red.

B. Reactively Loaded SIW Phase Shifter for Fine Phase Steps

In the proposed phase shifter, fine changes in phase shift are realized by introducing reactive loading into the waveguide. Reactive loading is introduced by filling dedicated drill holes, termed fine tuning vias, with liquid metal. The proposed phase

shifter incorporates a total of six fine tuning vias. In Fig. 1(b) the fine tuning vias are labelled P1 to P6. The fine tuning vias behave as inductive posts that modify the propagation of EM waves inside the SIW. The amount of phase shift provided by each tuning via can be controlled by the dimensions and the position of the via. In the proposed phase shifter, the fine tuning vias enable the phase shift to be varied from 0° to −60° in steps of 10°. In this way, fine tuning of the phase is enabled within each of the coarse steps of phase control. The design parameters of the proposed phase shifter are: the overall width of the phase shifter (W), the length of the longer folded section of SIW (L_1), the length of the longer folded section of SIW (L_1), the overall length of the phase shifter (L), the length of the shorter folded section of SIW (L_2), the length of the microstrip to SIW transition (T_L), the distance between the edge of SIW and the first LM tuning via (d), the width of the microstrip to SIW transition (T_W), the distance between fine tuning vias and the center of the SIW (d_1), the width of the SIW transmission line (a), the distance between adjacent fine tuning vias (d_2), the length of the initial section of SIW (L_2), the diameter of liquid metal fine tuning vias (L_{D2}), the width of the folded sections of SIW (W_1), the diameter of the matching vias (L_{D1}), the diameter of liquid metal vias used in the RF blocking walls and for the fine tuning vias (L_D), the distance between matching vias m_1 and m_3 and the corner of the SIW (S_1) and the distance between matching vias m_2 and m_4 and the corner of the SIW (S_2). Table I gives the dimensions of the proposed phase shifter.

TABLE I
THE DIMENSION OF THE PROPOSED PHASE SHIFTER (UNIT: MM)

$W = 56.2$	$L_1 = 17.43$	$d_2 = 6.3$	$L_2 = 19.24$
$L = 87.2$	$L_2 = 19.24$	$L_{D2} = 1$	$W_1 = 26.23$
$T_L = 5.1$	$d = 3$	$L_{D1} = 1.1$	$L_D = 1.2$
$T_W = 3.5$	$d_1 = 4.17$	$S_1 = 11.7$	$S_2 = 11.8$
$a = 13$			

III. DESIGN OF THE SIW PHASE SHIFTER

This section of the paper discusses the design process for the proposed phase shifter. The desired phase shift is achieved by combining both coarse and fine phase shifts, as mentioned earlier. The SIW phase shifter, reported in this paper, is designed to operate at 10 GHz; however, the design could readily be scaled to higher frequencies, e.g. millimeter. The phase shifter is designed around a Rogers RO4003C substrate, which has a dielectric constant (ε_r) = 3.55, a loss tangent ($tan\delta$) of 0.0027, and a thickness (h) of 0.813mm.

The dimensions of the SIW were determined by using the design process described in [35]-[37]. The width (a) of the SIW controls the cut-off frequencies (F_C) of the TE$_{10}$ and TE$_{20}$ modes of the waveguide. These modes constitute the lower and upper cut-off frequencies of the waveguide, and they are chosen to be 6.56 GHz and 13.12 GHz, respectively. For a substrate integrated waveguide these cut-off frequencies can be calculated using (1) and (2).

$$F_{C,mn} = \frac{c}{2\sqrt{\varepsilon_r}} \sqrt{\left(\frac{m}{a}\right)^2 + \left(\frac{n}{b}\right)^2} \tag{1}$$

$$F_{C,m0} = \frac{mc}{2a\sqrt{\varepsilon_r}} \tag{2}$$

Where: m and n are integers, b is the height of SIW, and c is the speed of light in a vacuum.

For convenience, SMA connectors are employed at both ends of the phase shifter. To facilitate this, it was necessary to design a transition from SIW to microstrip and add that transition to each end of the SIW structure. The transition was designed using the process described in [36], [38]. The length (TL) and width (TW) of the tapered transition were optimized by using the Frequency Domain Solver in CST Microwave Studio® 2019, in order to yield an S$_{11}$ below -15 dB over the operating bandwidth of the SIW line.

A. Switched Line SIW Phase Shifter for Coarse Phase Steps

The large (i.e. coarse) changes in phase are achieved by using a switched-line phase shifter, as mentioned earlier. The switched-line phase shifter was designed to produce three different phase-shift values, namely -60°, -120° and -180°. This was achieved by adjusting the physical length of the SIW line.

Let us now consider, what happens when the drill holes are not filled with liquid metal, but with air instead, which has the effect of altering the guided wavelength. Those drill holes are associated with the matching vias and the blocking walls. A series of small correction factors are needed to account for the effect of these air-filled drill holes on the guided wavelength. The correction factors were determined through computer simulations in CST Microwave Studio. The correction factor for state A (c_a) is 0.36 mm, whereas, this factor for state B (c_b) and C (c_c) is 0.73 mm. The correction factors for states B and C are larger than that for state A, owing to the existence of more empty vias in the path of EM waves.

Depending on the length of the SIW line, it was either configured into a straight or folded path (see Figs. 1 and 2). At 10 GHz, the guided wavelength λ_g within the SIW line is 21 mm. The first path, shown in Fig. 2(a), pertains to state A. In this state, the line is designed to have an average physical length $L_A = 3\lambda_g + \lambda_g/6 + c_a$, which evaluates to 63 + 3.5 + 0.36 = 66.86 mm, or −1140°. This corresponds to a phase shift of −60° at 10 GHz. The second path, shown in Fig. 2(b), corresponds to state B. The line is designed to have an average physical length $L_B = 2(L_A/2 − a/2) + 2L_V + L_h + c_b = 4\lambda_g + 2(\lambda_g/6) + 0.73$ mm. This evaluates to 84 + 2×3.5 + 0.73 = 91.73 mm, or −1560°. This corresponds to a relative phase shift of −120° at 10 GHz. The third path, shown in Fig. 2(c), pertains to state C. It is designed to have an average physical length $L_C = (L_A/2 − a/2) + 2L_{V1} + L_{h1} + c_c = 4\lambda_g + 3(\lambda_g/6) + 0.73$ mm. This evaluates to 84 + 3 × 3.5 + 0.73 = 95.23 mm, or −1620°. This corresponds to a phase shift of −180° at 10 GHz. (3)-(5) below summarize the lengths of the three main paths:

$$L_A = 3\lambda_g + \lambda_g/6 + c_a \tag{3}$$

$$L_B = 2(L_A/2 − a/2) + 2L_V + L_h + c_b \tag{4}$$

$$L_C = 2(L_A/2 − a/2) + 2L_{V1} + L_{h1} + c_c \tag{5}$$

An individual via is said to be ON or OFF, depending on whether it is filled with, or emptied of, liquid metal. Each blocking wall is formed from a row of holes drilled into the substrate. When all of the holes associated with a particular wall are filled with liquid metal, that wall is said to be turned ON. The individual paths within the switched-line phase shifter can be opened or closed independently, by adding or removing the relevant blocking walls. In Fig. 1, the blocking walls are labeled G_1 to G_5. A third set of vias, termed the matching vias, are used to improve the impedance matching associated with the different paths. Those vias are labelled m_1 to m_4. Table II details the configuration of the various walls and matching vias required to realize each operating state. For example, if G_1, G_2, G_3 and G_4 are switched ON, while G_5, m_1 to m_4, and P_1 to P_6 are switched OFF, the EM waves are confined in the central section of the SIW line and a phase shift of -60° is realized, as shown in Figs. 1(a) and 1(d).

TABLE II
THE RELATIONSHIP BETWEEN ACTIVE VIAS AND THE CONFIGURATION OF MAIN THREE PATHS OF THE PROPOSED PHASE SHIFTER

State	Vias ON	Phase Shift (°)
A	G_1, G_2, G_3, G_4	-60
B	G_4, G_3, G_5, m_2 and m_4	- 120
C	G_1, G_2, G_5, m_1 and m_3	- 180

B. Reactively Loaded SIW Phase Shifter for Fine Phase Steps

The small (i.e. fine) changes in phase are achieved by altering the reactive loading within the SIW line, which is achieved by activating/deactivating one or more of the dedicated fine tuning vias that are located adjacent to the via walls. These vias are labeled P_1 to P_6, and they can be used to control the phase in steps of 10°. P_1 to P_3 are added at the input of the phase shifter, while P_4 to P_6 are added at its output, as shown in Fig. 2(b). Each via is inset, from the side walls of the SIW, by a small distance, denoted d_1. The concept and the experimental validation, of this approach, was presented in detail in [39]-[40]. In summary, the vias constitute an inductive loading within the SIW line which modifies the phase of the EM waves. Each metallic via can be modeled by using a lumped-element equivalent circuit consisting of a T-network of components that acts as a high-pass filter and thus leads to a phase advance. The T-network incorporates a shunt inductance and two series capacitances. When the diameter of the via is much less than the width of the SIW line (a), the T-network reduces to a single shunt inductance [39]-[40]. For this reason, the value of the phase shift varies as a function of the via diameter and the inset of the vias with respect to the side walls of the SIW (denoted S_2) [39]. Furthermore, it has been shown that displacing a via in the y-direction (i.e. altering d_1) controls the phase shift which it provides, whilst displacing a via in the x-direction controls the return loss. By controlling these parameters, a phase shift of up to 75° has been demonstrated using a single via [39]. In the proposed design, the minimum phase shifting step was set to 10°, as mentioned earlier. This was achieved by optimizing the: diameter, separation between neighboring vias, and the inset of the vias from the waveguide centre d_1, based on the criterion presented in [39]-[41]. The smallest phase step that could be achieved in this way is 1.2°. In order to achieve this, it would

be necessary to reduce either S_2 or the diameter of the vias [40]. Using vias with smaller diameters would reduce the reactive loading and, consequently, reduce the achieved phase shift; additionally, it would improve the quality of the impedance matching. However, if the phase-shifting step were reduced, then a larger number of vias would be required to achieve the same overall phase shifting range. Also it would be more difficult to fill closely separated vias with liquid metal; consequently, the fabrication complexity would increase. Considering all of the aforementioned issues, a 10° phase shift was chosen to obtain a good trade-off between phase shift and insertion loss.

The design procedure of the proposed phase shifter can be summarized as follows:

1. Use (1) to (2) to determine the dimensions of the SIW transmission lines.
2. Design a simple straight SIW path having a length of L_A to achieve a phase shift of -60°.
3. Design two folded paths, having lengths of L_B and L_C, to achieve phase shifts of -120° and -180°, respectively.
4. Optimize the position of the four matching vias, located in the corners of each folded path. The objective is to keep the width of the waveguide roughly constant throughout the folded section. The positions of the matching vias (e.g. m_1) can be determined by drawing a diagonal line (placed at an angle $\theta = 45°$ to the verticle) and then translating the appropriate corner via along that diagonal, through a specified distance (e.g. S_1), shown in Fig. 2(c). The parameters S_1 and S_2 must be optimized to improve the matching (i.e. S_{11} and S_{22}, respectively). Matching via m_3 is the mirror image of m_1, while m_4 is the mirror image of m_2. For this reason, their position is determined by a process analogous to the one described above.
5. Design the first fine tuning via (i.e. P_1) to achieve the desired phase tuning step (in this case 10°). The phase tuning step is controlled by d_1. The distance between the edge of the SIW and the first fine tuning via (i.e. d) has no effect on the phase tuning step.
6. The distance between first tuning via P_1 and second tuning vias P_2 (i.e. d_2) affects the matching of the phase shifter but has negligible effect on the phase. Optimize d_2 to keep S_{11} and S_{22} below -15 dB.
7. Add the third tuning via (i.e. P_3) at a distance d_2 (obtained in the previous step) from the second tuning via (i.e. P_2).
8. Add tuning vias P_4 to P_6 to the output of the phase shifter. Please note that P_4 to P_6 are the identical mirror image of P_1 to P_3 and thus they are designed by following steps 5 to 7.
9. Include the fine tuning vias in the phase shifter and optimize the final structure to obtain the desired phase shifts.
10. Design the taper for the SIW to microstrip line transition and simulate the entire structure including

the SMA connectors.

IV. PRACTICAL FABRICATION CONSIDERATIONS

This section of the paper discusses the fabrication and actuation of the hardware prototype, shown in Fig. 3. The channel structure, used to contain and guide the liquid metal, consists of two layers of clear Perspex. In Fig. 3, these layers are labelled layer 1 (#L_1) and layer 2 (#L_2). Each layer incorporates several liquid metal reservoirs (LMRs). The layers of Perspex were held in place using 12 metallic screws which were located outside the SIW. A syringe was used to inject or remove liquid metal from each via. This approach for actuation is commonly employed in the literature [30], [42]-[51]. Alternative methods of actuation have been reported in the literature, including electrochemically controlled capillary action [52]-[53] and the use of a micropump [21], [54]-[57]. One of these existing techniques could be employed in this application. However, liquid metal actuation is not the main focus of this paper. Moreover, altering the method of actuation would have minimal effect on the RF performance of the proposed phase shifter because the actuation circuits would be located beneath the ground plane, where the electric and magnetic field strengths are minimal. In our experiments, no residues of liquid metal were observed inside the vias after the liquid metal was removed. The proposed phase shifter was actuated several times in order to test its repeatability. The performance was largely unchanged. Typically, the same batch of liquid metal was reused over and over again in the experiments. Once again, this was found to have negligible effect on the RF performance.
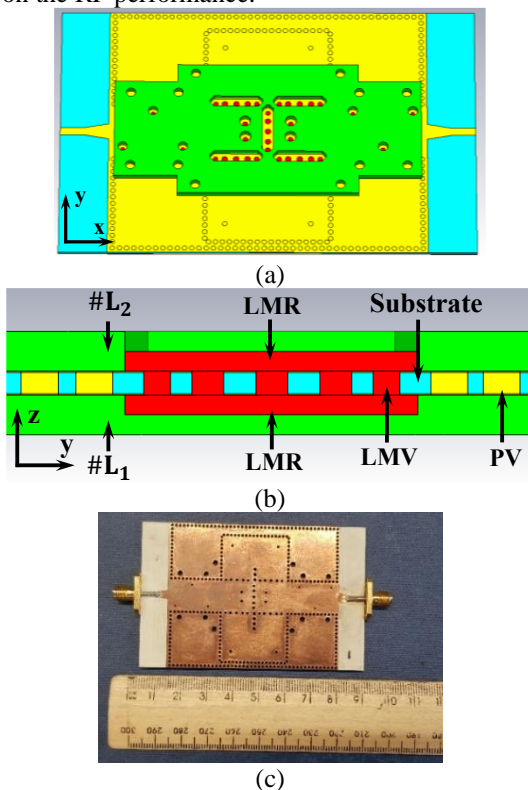

(a)

(b)

(c)

Fig. 3. The proposed phase shifter with Perspex cover. (a) top view and (b) cross section of z-y plane and (c) fabricated prototype. Key: #L_1 = Perspex Layer 1, #L_2 = Perspex layer 2, LMR = Liquid metal reservoir, LMV = Liquid metal via, PV = Copper plated via, Substrate = blue, Perspex = Green, Copper plated vias = yellow, Liquid metal vias = red.
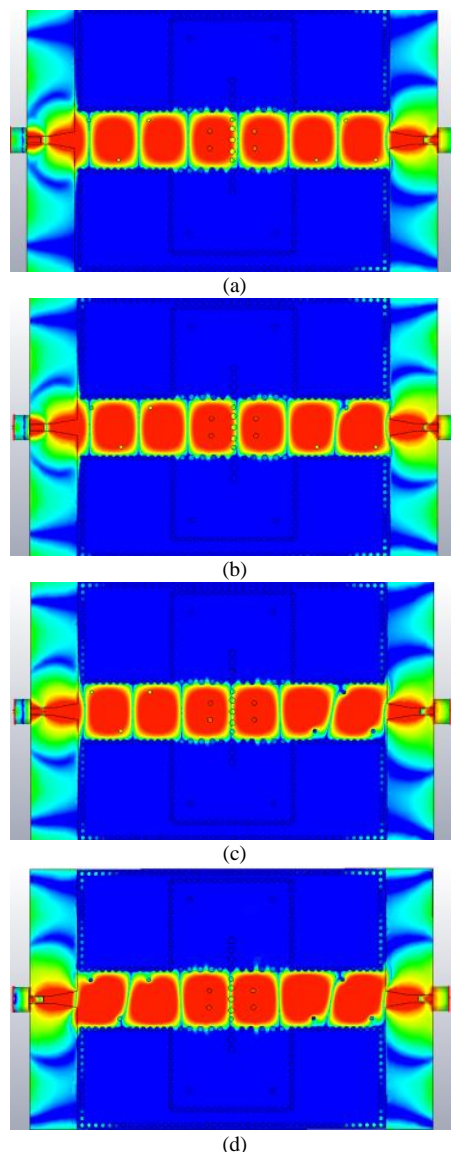

(a)

(b)

(c)

(d)

Fig. 4. The effect of tuning vias on the E-field of the proposed phase shifter at 10 GHz. (a) P_1 to P_6 are OFF, (b) P_2 only is ON, (c) P_1 to P_3 are ON, and (d) P_1 to P_6 are ON.

V. RESULTS AND DISCUSSION

Fig. 4 shows the simulated electric field (E-field) distribution, associated with state A of the proposed phase shifter. Fig. 4(a) shows the structure with no fine tuning vias activated. Fig. 4(b) shows the structure with one fine tuning via activated (namely P_2). Fig. 4(c) shows the structure with three fine tuning vias (namely: P_1 to P_3) activated. Fig. 4(d) shows the structure with six fine tuning vias (P_1 to P_6) activated. It can be observed that the fine tuning vias perturb the propagating EM waves, and therefore their associated phase shift. Table III details the configuration of the various walls and matching vias required to realize each operating state, along with the associated phase shift. It is important to mention that any combination of the six different vias (viz. P_1 to P_6) could be switched ON in order to obtain any particular 10° increment in the phase shift. In other words, the phase shift is determined by the number of vias that are turned ON, rather than by the positions of those vias. Table

III describes just one possible solution, although it is worthwhile mentioning here, that several other permutations are also possible.

TABLE III
PHASE SHIFTER SCHEME

Phase shift (°)	Coarse vias ON		Matching Vias ON	Small vias ON
0	State A	G_1 to G_4	None	P_1 to P_6
-10		G_1 to G_4	None	P_1 to P_5
-20		G_1 to G_4	None	P_1 to P_4
-30		G_1 to G_4	None	P_1 to P_3
-40		G_1 to G_4	None	P_1 to P_2
-50		G_1 to G_4	None	P_1
-60		G_1 to G_4	None	None
-60	State B	G_3 to G_5	m_2 and m_4	P_1 to P_6
-70		G_3 to G_5	m_2 and m_4	P_1 to P_5
-80		G_3 to G_5	m_2 and m_4	P_1 to P_4
-90		G_3 to G_5	m_2 and m_4	P_1 to P_3
-100		G_3 to G_5	m_2 and m_4	P_1 to P_2
-110		G_3 to G_5	m_2 and m_4	P_1
-120		G_3 to G_5	m_2 and m_4	None
-120	State C	G_1, G_2 and G_5	m_1 and m_2	P_1 to P_6
-130		G_1, G_2 and G_5	m_1 and m_2	P_1 to P_5
-140		G_1, G_2 and G_5	m_1 and m_2	P_1 to P_4
-150		G_1, G_2 and G_5	m_1 and m_2	P_1 to P_3
-160		G_1, G_2 and G_5	m_1 and m_2	P_1 to P_2
-170		G_1, G_2 and G_5	m_1 and m_2	P_1
-180		G_1, G_2 and G_5	m_1 and m_2	None

TABLE IV
MEASURED PHASES OF THE PROPOSED PHASE SHIFTER

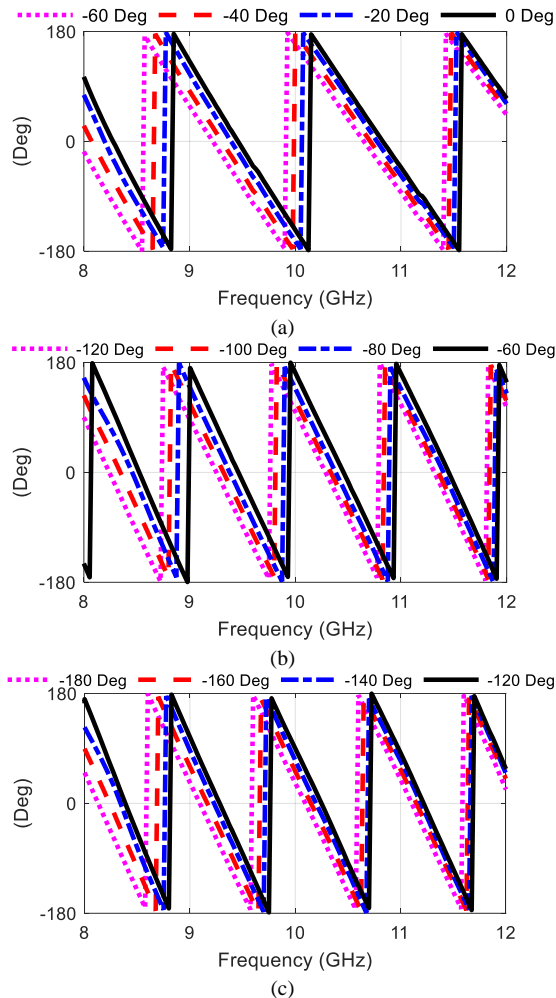| Simulated Phase shift	Measured Phase shift	Step difference Measured
0°	0°	0
-10°	-8.4°	8.4
-20°	-18.6°	10.2
-30°	-27.7°	9.1
-40°	-37.1°	9.4
-50°	46.1°	9
-60°	55.3°	9.2
-60°	62.0°	-
-70°	68.7°	6.7
-80°	77.2°	8.5
-90°	88.5°	11.3
-100°	96.5°	8.0
-110°	105.8°	9.3
-120°	115.4°	9.6
-120°	124.1°	-
-130°	133.9°	9.8
-140°	143.5°	9.6
-150°	152.9°	9.4
-160°	161.4°	8.5
-170°	171.0°	9.6
-180°	181.1°	10.1

Fig.5. The measured S_{21} phase response of the all cases of the of the proposed phase shifter. (a) (state A: 0° to -60°) (b) (state B: -60° to -120°) and (c) (state C: -120° to -180°).

Fig. 5 shows the phase of S_{21} for the proposed phase shifter, in each of the three main operating states. The measured and simulation results are seen to be in very good agreement, with the results predicting a phase difference of 60° between each of the three main states. The calibration of the measured device was performed using Through, Reflect, Line (TRL) approach. The calibration kit was an electronic kit provided by Keysight. The simulated and measured insertion loss values provided in the paper include the losses within the SMA connectors. Also, phase stable cables were used during the measurements. The phase shifter itself was fabricated on a rigid substrate which did not flex during the measurements. These factors negate the requirement for a test fixture.

At 10 GHz, the measured phase difference between states A and B is 62.0°, while this difference is 62.1°, between states B and C. In addition, according to simulation, the smallest available phase shift, within each of the three coarse phase steps, is 10°. The measurement results are summarized in Table IV. Table IV shows that the measured phase step for the proposed phase shifter ranges from 8.4° to 11.3°, which is in good agreement with the simulated steps of 10°. This
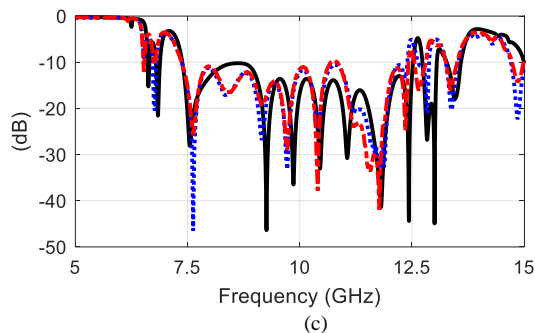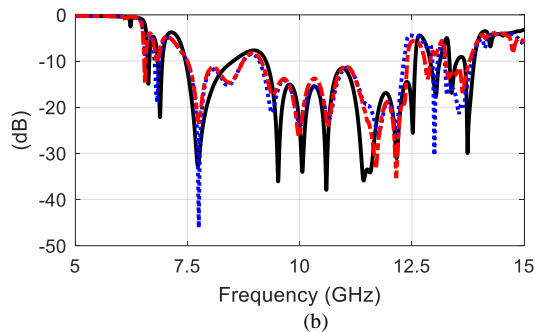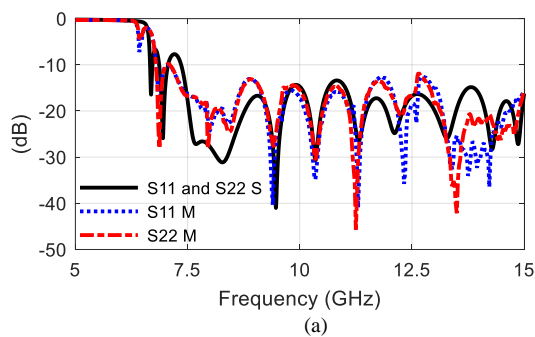
Fig. 6. Measured and simulated S11 and S22 of the main three states of the proposed phase shifter. (a) State A (-60°), (b) State B (-120°), and (c) State C (-180°). Key: S in the figure stands for simulated and M stands for measured.

Fig. 7. Measured and simulated S_{21} and S_{12} of the main three states of the proposed phase shifter. (a) state A (-60°) (b) state B (-120°) and (c) state C (-180°). Key: S in the figure stands for simulated and M stands for measured.

effectively means that the phase can be tuned from 0° to 180° in steps of 10°.

Figs. 6 to 9 show the measured S-parameters for the proposed phase shifter. Fig. 6 shows the reflection coefficients (S_{11} and S_{22}) associated with the three main states of the phase shifter. It can be observed that the phase shifter has a measured -10 dB bandwidth of at least 5 GHz ranging from 7.5 GHz to 12.5 GHz. Fig. 7 shows S_{21} and S_{12} for the three main operating states of the phase shifter. The measured insertion loss for the three operating states ranges from 1.2 dB to 2 dB at 10 GHz. Figs. 8 and 9 show the S_{11} and the S_{21} of the proposed phase shifter when the fine tuning vias are activated. For all cases, the phase shifter has a measured -10 dB bandwidth of more than 3.5 GHz ranging from 8.5 GHz to 12 GHz, with a measured insertion loss ranging from 1.2 dB to 2.3 dB, as shown in Figs. 7 and 9. The insertion losses are only due to dissipation losses and matching losses. The simulation results indicate that the insertion loss could be decreased by an additional ∼0.5 dB, if a substrate material with a lower dissipation loss was used, such as RT5880 (RT5880 has a loss tangent of 0.0009, compared with 0.0027 for RO4003C).
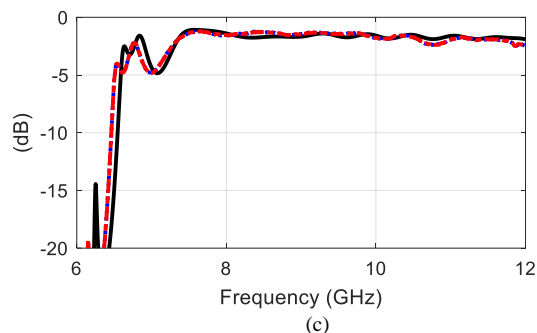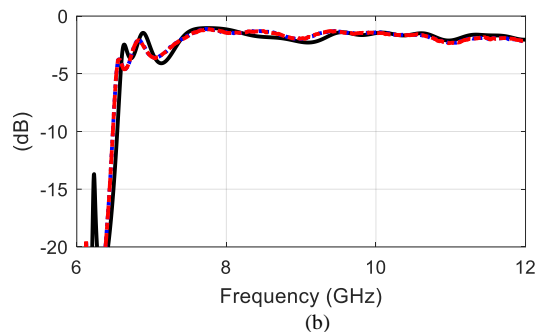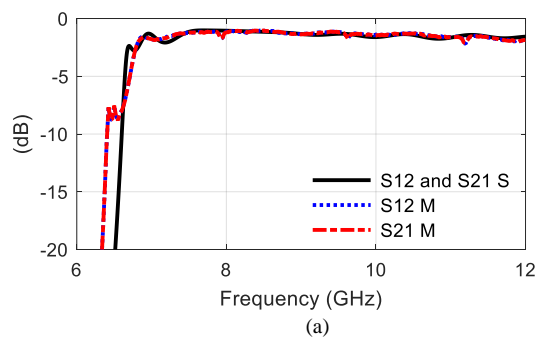
Fig. 10 shows the difference in phase between each of the main operating states of the proposed phase shifter. At the operating frequency (i.e. 10 GHz) the phase difference between successive states (e.g. A and B) should be 60°. The curves, shown in Fig. 10, have been normalized so that the phase difference at 10 GHz is set to 0°. The normalized phase difference is plotted, as a function of frequency, over the 2 GHz (i.e. 9 GHz to 11 GHz) operating bandwidth of the phase shifter. Consider the curves depicting the normalized phase difference between state B relative to state A, and state C relative to state A. For these curves the phase fluctuates by less than ±5° over a measured absolute bandwidth of ∼160 MHz. For a phase flatness of ±10° the absolute bandwidth is ∼260 MHz, and for a phase flatness of ±20° the absolute bandwidth is ∼520 MHz. These states exhibit the worst performance in terms of phase flatness. The overall limit on the bandwidth of the phase shifter for a given value of phase flatness is set by those states having the worse performance. Let us now consider the root mean square (RMS) bandwidth of the phase shifter. Again we will consider the state B relative to state A and state C relative to state A. For a phase flatness of ±5°, the proposed phase shifter
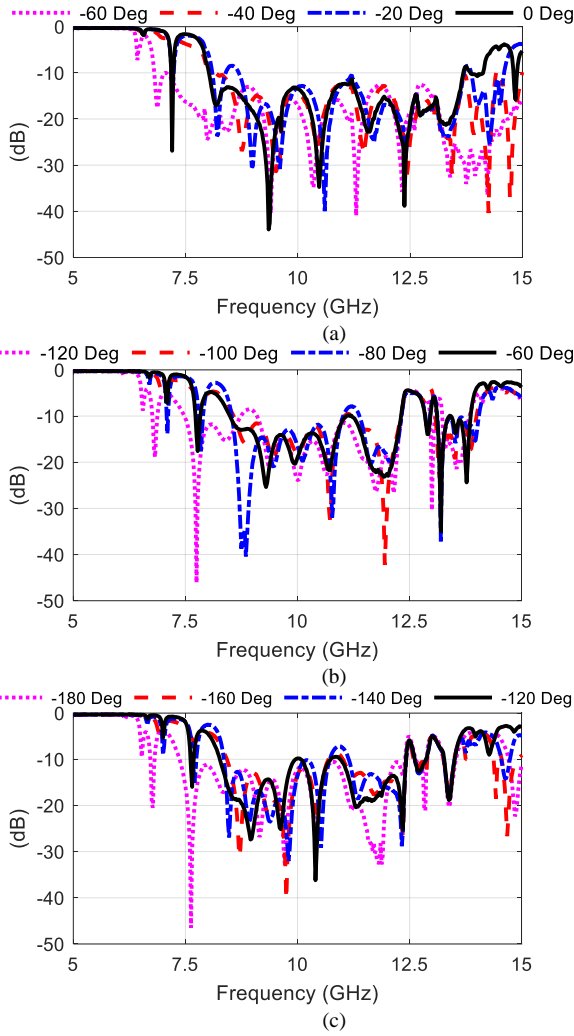
Fig. 8. The measured S_{11} of selected cases of the proposed phase shifter. (a) (0° to -60°) (b) (-60° to -120°) and (c) state C (-120° to -180°).

Fig. 9. The measured S_{21} of selected cases of the proposed phase shifter when the fine tuning vias are active. (a) (state A: 0° to -60°) (b) (state B: -60° to -120°) and (c) (state C: -120° to -180°).

Fig. 10. Normalized change in the phase of the phase shifter over the operation bandwidth.

has an RMS bandwidth of ~230MHz. For a phase flatness of ±10° the RMS bandwidth is ~440MHz. Finally, for a phase flatness of ±20° the RMS bandwidth is ~1 GHz. It is evident, therefore that, in all cases the RMS bandwidths are larger than the absolute bandwidths. Now let us consider the normalized phase difference between state C relative to state B. It can be seen that, for this curve, the bandwidth for a given value of phase flatness is better than that for the other two curves. The reason for this is that the phase shifts of -120° (for state B) and -180° (for state C) were obtained by using a waveguide having an electrical length which is several multiple of $4\lambda_g$ long (i.e. -4×360°-120° and -4×360°-180°, respectively), whereas the phase shift of -60° (for state A) was instead obtained by using a waveguide having an electrical length which is several multiple of $3\lambda_g$ long (i.e. -3×360°-60°). We can therefore see that the electrical lengths of the waveguide for states B and C are quite similar to each other.

Finally, let us now consider the reactively loaded SIW phase shifter that can be used to achieve fine control of the phase (-10° per tuning via). The change of the electrical length created by each tuning via (P1 to P6) alone is very small (-10° per tuning via). This yields a relatively wide operating bandwidth,
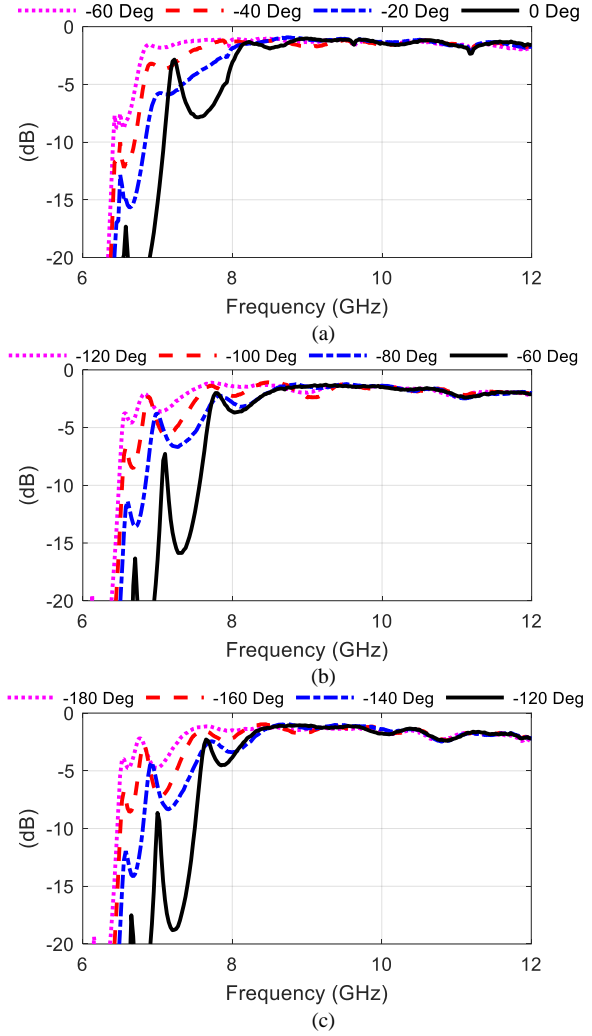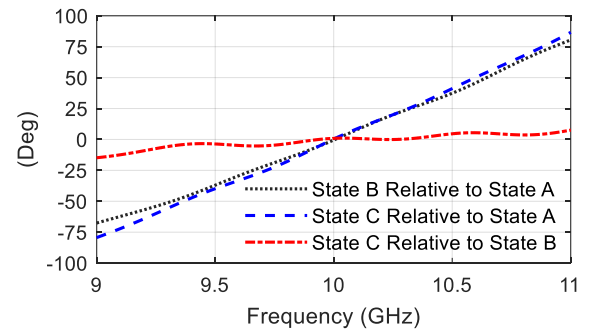
within each of the three main states. Consequently, for each of the fine steps of phase tuning, within states B and C, the proposed phase shifter exhibits a much wider bandwidth for a given value of phase flatness. Fig. 10 shows that the worst absolute bandwidths (pertaining to the fine phase shifts) are: ~600 MHz for a phase flatness of ± 5°, ~1.3 GHz for a phase flatness of ±10°, and ~2.3 GHz for a phase flatness of ±20°. Once again, the RMS bandwidth values are much larger.

Table V presents a comparison of the performance of the

TABLE.V
PERFORMANCE COMPARISON OF DIFFERENT PHASE SHIFTERS THAT OPERATE AT X-BAND WITH CENTER FREQUENCY AT ~10 GHZ.

	This Work	[58]	[59]	[60]	[61]	[62]	[63]	[64]
Technology	Liquid Metal	GaN-HEMT	CMOS-13μm	LTCC-Ferrite	PCB-Varactor Diode	LTCC-Ferrite	SIW- PIN Diode	PCB-Ferrite
Phase resolution (bit/deg.)	10°	5 bits (11.25°)	6 bit (5.625°)	NA	NA	NA	NA	50°
Phase shifting Range	0 -180°	0 -180°	0 -360°	0 -216°	0 -392°	0 -166.4°	0 -180°	0 -200°
Insertion loss (dB)	1.2 – 2.3	14	>11	3.4 – 6.3	3.3	≈ 2.5	≈ 2	≈ 3.5
Input return loss (dB)	≈15	7.6	≈14	<10	>10	<10	<15	<12
Output return loss (dB)	≈15	6.5	≈12	<10	NA	<10	<15	NA
Bandwidth (GHz)	≈0.44	≈3	≈3	NA.	2	0.6	4	NA
RMS phase error (Deg.)	10°	6°	4.9°	NA	NA	NA	NA	NA
Size (mm)	56.2 × 87.2	5 × 4.7	2.6 × 0.6	20 × 20	NA	4 × 15	NA	51 × 25

proposed phase shifter against that of other state-of-the-art phase shifters. Each column in the table presents the performance of a different, competing category of phase shifting technology. The references were selected because they describe designs whose performance level is typical of phase shifters within that category of technology. There are no papers, in the existing literature, on SIW phase shifters that can be reconfigured by using liquid metal. The proposed phase shifter has several advantages in comparison with competing technologies. Those advantages include: (i) bidirectional and reciprocal operation; (ii) very low insertion loss considering the resolution of phase control available, which is 10°; and (iii) potential for improved power handling. The latter derives from the fact that SIW has good power handling capabilities and so one would expect the same of the structure proposed in this paper as there would appear to be nothing about liquid metal that should inherently limit its power handling capability. Disadvantages of the proposed phase shifter include relatively low switching speed and relatively large size. Currently the switching speed of the proposed device (expected to range from seconds to milliseconds [12], [34]) is likely to be lower than that of competing devices. Liquid metal actuation speeds of up to 30cm/s have been reported in the literature [65]. However, with further developments, actuation speeds are likely to increase. The actuation speed depends on the volume of LM which we wish to move. Actuating a via involves moving a tiny volume of LM (sub-μL) and so high speeds may be possible.

VI. Conclusion

This paper presents the first phase shifter, based around substrate integrated waveguide (SIW) technology, that can be reconfigured using liquid metal. The phase shifter operates at 10 GHz and exhibits low insertion loss. Phase shifting is achieved by using a combination of coarse and fine phase tuning, which enables the proposed phase shifter to achieve a phase shift ranging between 0° and 180°, in steps of 10°. The coarse phase shift is realized by reconfiguring between three different SIW paths, having different electrical lengths, to

achieve phase shifts of 60°, 120° and 180°. Reconfiguration between these paths is achieved by adding/removing RF blocking walls. Each wall consists of group of liquid metal vias. Furthermore, six fine tuning vias formed from liquid metal were used for to achieve fine control over the phase using the mechanism of reactive loading. Measured and simulated results, provided in the paper, serve to demonstrate that the performance of the proposed phase shifter is satisfactory. It achieves a measured phase shift of up to 180° in approximately 10° phase steps, and it has a low insertion loss. The proposed phase shifter will be applicable within a wide range of different reconfigurable microwave devices.

References

[1] S. Hayden and G. M. Rebeiz, "2-bit MEMS distributed X-band phase shifters," *IEEE Microw. Guided Wave Lett.*, vol. 10, no. 12, pp. 540-542, Dec. 2000.

[2] A. E. Martynyuk, A. G. Martinez-Lopez and J. I. Martinez Lopez, "2-bit X-Band Reflective Waveguide Phase Shifter with BCB-Based Bias Circuits," *IEEE Trans. Microw. Theory Techn.*, vol. 54, no. 12, pp. 4056-4061, Dec. 2006.

[3] B. T. W. Gillatt, M. D'Auria, W. J. Otter, N. M. Ridler and S. Lucyszyn, "3-D Printed Variable Phase Shifter," *IEEE Microw. Wireless Compon. Lett.*, vol. 26, no. 10, pp. 822-824, Oct. 2016.

[4] J. J. P. Venter, T. Stander and P. Ferrari, "X-Band Reflection-Type Phase Shifters Using Coupled-Line Couplers on Single-Layer RF PCB," *IEEE Microw. Wireless Compon. Lett.*, vol. 28, no. 9, pp. 807-809, Sept. 2018.

[5] M. A. Morton, J. P. Comeau, J. D. Cressler, M. Mitchell and J. Papapolymerou, "5 bit, silicon-based, X-band phase shifter using a hybrid pi/t high-pass/low-pass topology," *IET Microw. Ant. & Propag.*, vol. 2, no. 1, pp. 19-22, Feb. 2008.

[6] Y. Du, J. Bao and X. Zhao, "5-bit MEMS distributed phase shifter," *IET Electr. Lett.*, vol. 46, no. 21, pp. 1452-1453, Oct. 2010.

[7] Guan-Leng Tan, R. E. Mihailovich, J. B. Hacker, J. F. DeNatale and G. M. Rebeiz, "A 2-bit miniature X-band MEMS phase shifter," *IEEE Microw. Wireless Compon. Lett.*, vol. 13, no. 4, pp. 146-148, Apr. 2003.

[8] K. Gharibdoust, N. Mousavi, M. Kalantari, M. Moezzi and A. Medi, "A Fully Integrated 0.18 CMOS Transceiver Chip for X-Band Phased-Array

Systems," *IEEE Trans. Microw. Theory Techn.*, vol. 60, no. 7, pp. 2192-2202, Jul. 2012.

[9] M. Cho, D. Baek and J. Kim, "An X-Band 5 Bit Phase Shifter With Low Insertion Loss in 0.18μm SOI Technology," *IEEE Microw. Wireless Compon. Lett.*, vol. 22, no. 12, pp. 648-650, Dec. 2012.

[10] T. N. Ross, K. Hettak, G. Cormier and J. S. Wight, "Design of X-Band GaN Phase Shifters," *IEEE Trans. Microw. Theory Techn.*, vol. 63, no. 1, pp. 244-255, Jan. 2015.

[11] W. Luo, H. Liu, Z. Zhang, P. Sun and X. Liu, "High-Power X -Band 5b GaN Phase Shifter With Monolithic Integrated E/D HEMTs Control Logic," *Electron Devices*, vol. 64, no. 9, pp. 3627-3633, Sept. 2017.

[12] A. Qaroot and G. Mumcu, "Microfluidically Reconfigurable Reflection Phase Shifter," *IEEE Microw. Wireless Compon. Lett.*, vol. 28, no. 8, pp. 684-686, Aug. 2018.

[13] S. Yeo, J. Chun and Y. Kwon, "A 3-D X-Band T/R Module Package with an Anodized Aluminum Multilayer Substrate for Phased Array Radar Applications," *IEEE Trans. Adv. Packag.*, vol. 33, no. 4, pp. 883-891, Nov. 2010.

[14] S. Sim, L. Jeon and J. Kim, "A Compact X-Band Bi-Directional Phased-Array T/R Chipset in 0.13 μm CMOS Technology," *IEEE Trans. Microw. Theory Techn.*, vol. 61, no. 1, pp. 562-569, Jan. 2013.

[15] C. Chang *et al.*, "A New Compact High-Power Microwave Phase Shifter," *IEEE Trans. Microw. Theory Techn.*, vol. 63, no. 6, pp. 1875-1882, Jun. 2015.

[16] B. Acikel, T. R. Taylor, P. J. Hansen, J. S. Speck and R. A. York, "A new high performance phase shifter using Ba/sub x/Sr/sub 1-x/TiO3 thin films," *IEEE Microw. Wireless Compon. Lett.*, vol. 12, no. 7, pp. 237-239, Jul. 2002.

[17] S. Kagita, A. Basu and S. K. Koul, "Characterization of LTCC-Based Ferrite Tape in X-band and Its Application to Electrically Tunable Phase Shifter and Notch Filter," *IEEE Trans. Magn.*, vol. 53, no. 1, pp. 1-8, Jan. 2017.

[18] Zhang Jin, S. Ortiz and A. Mortazawi, "Design and performance of a new digital phase shifter at X-band," *IEEE Microw. Wireless Compon. Lett.*, vol. 14, no. 9, pp. 428-430, Sept. 2004.

[19] D. J. Chung, R. G. Polcawich, J. S. Pulskamp and J. Papapolymerou, "Reduced-Size Low-Voltage RF MEMS X-Band Phase Shifter Integrated on Multilayer Organic Package," *IEEE Trans. Compon., Packag. and Manuf. Technol.*, vol. 2, no. 10, pp. 1617-1622, Oct. 2012.

[20] R. Ramadoss, A. Sundaram and L. M. Feldner, "RF MEMS phase shifters based on PCB MEMS technology," *IET Elect. Lett.*, vol. 41, no. 11, pp. 654-656, May 2005.

[21] Sarah N. McClung, Shahrokh Saeedi, Hjalti H. Sigmarsson, "Band-Reconfigurable Filter With Liquid Metal Actuation," *IEEE Trans. Microw. Theory Techn.*, vol. 66, no. 6., pp. 3073-3080. Jun. 2018.

[22] Jonathan H. Dang, Ryan C. Gough, Andy M. Morishita, Aaron T. Ohta, Wayne A. Shiroma, "A Tunable X-Band Substrate Integrated Waveguide Cavity Filter using Reconfigurable Liquid-Metal Perturbing Posts," in *IEEE MTT-S Int. Microw. Symp. (IMS)*, 2015.

[23] Sarah N. McClung, Shahrokh Saeedi, Hjalti H. Sigmarsson, "Single-Mode-Dual-Band to Dual-Mode-Single-Band Bandpass Filter with Liquid Metal," in Proc. *IEEE 18th Wireless and Microw. Technol. Conference (WAMICON)*, 2017.

[24] Alex H. Pham, Shahrokh Saeedi, Hjalti H. Sigmarsson, "Continuously-Tunable Substrate Integrated Waveguide Bandpass Filter Actuated by Liquid Metal," in Proc. *IEEE MTT-S Int. Microw. Symp. (IMS)*, 2019.

[25] Tahar Ben Chaieb, Abdelkhalek Nasri, Hassen Zairi, "Liquid filled method for Substrate Integrated Waveguide reconfigurable filter," in Proc. *Int. Conference on Adv. Sys. and Electric Technol. (IC_ASET)*, 2018.

[26] Sabreen Khan, Nahid Vahabisani, Mojgan Daneshmand, "A Fully 3-D Printed Waveguide and Its Application as Microfluidically Controlled Waveguide Switch," *IEEE Trans. Compon., Packag. and Manuf. Technol.*, vol. 7, no. 1, pp. 70-80, Jan. 2017.

[27] Nahid Vahabisani, Sabreen Khan, Mojgan Daneshmand, "A K-Band Reflective Waveguide Switch Using Liquid Metal," *IEEE Antennas Wireless Propag. Lett.*, vol. 16, pp. 1788-91, Mar. 2017.

[28] S. Alkaraki, J. Kelly, A. L. Borja, R. Mittra and Y. Wang, "Gallium-Based Liquid Metal Substrate Integrated Waveguide Switches," *IEEE Microw. and Wireless Compon. Lett.*, vol. 31, no. 3, pp. 257-260, Mar. 2021.

[29] Meng Wang, Ian M. Kilgore, Michael B. Steer, Jacob J. Adams, "Characterization of Intermodulation Distortion in Reconfigurable Liquid Metal Antennas," *IEEE Antennas Wireless Propag. Lett.*, vol. 17, no. 2, pp. 279-82, Feb. 2018.

[30] Andy M. Morishita, Carolynn K. Y. Kitamura, Aaron T. Ohta, Wayne A. Shiroma, "A Liquid-Metal Monopole Array with Tunable Frequency, Gain, and Beam Steering," *IEEE Antennas Wireless Propag. Lett.*, vol. 12, no. pp. 1388-91, Oct. 2013.

[31] Cong Wang, Joo Chuan Yeo, Hui Chu, Chwee Teck Lim, Yong-Xin Guo, "Design of a Reconfigurable Patch Antenna Using the Movement of Liquid Metal," *IEEE Antennas Wireless Propag. Lett.*, vol. 17, no. 6, pp. 974-977, Jun. 2018.

[32] M. Wang, C. Trlica, M. R. Khan, M. D. Dickey, and J. J. Adams, "A reconfigurable liquid metal antenna driven by electrochemically controlled capillarity," *J. Appl. Phys.*, vol. 117, no. 19, May 2015.

[33] J. H. Dang, R. C. Gough, A. M. Morishita, A. T. Ohta and W. A. Shiroma, "Liquid-metal-based phase shifter with reconfigurable EBG filling factor," in Proc. *IEEE MTT-S Int. Microw. Symp.*, Phoenix, AZ, 2015, pp. 1-4.

[34] A. Dey and G. Mumcu, "Microfluidically Controlled Frequency Tunable Monopole Antenna for High-Power Applications," *IEEE Antennas Wireless Propag. Lett.*, vol. 15, pp. 226-229, 2016.

[35] Young, L. Yan, W. Hong, K. Wu, and T. J. Cui, "Investigations on the propagation characteristics of the substrate integrated waveguide based on the method of lines," *IEE Proc. Microw., Antennas and Propag.*, vol. 152, no. 1, pp. 35–42, Feb. 2005. Doi:10.1049/ip-map:20040726

[36] J. E. Rayas-Sanchez and V. Gutierrez-Ayala, " A general EM-based design procedure for single-layer substrate integrated waveguide interconnects with microstrip transitions," *2008 IEEE MTT-S Int. Microwave Symp. Digest*, Atlanta, GA, USA, 2008, pp. 983-986.

[37] Feng Xu and Ke Wu, "Guided-wave and leakage characteristics of substrate integrated waveguide," in *IEEE Trans. on Microw. Theory Techn.*, vol. 53, no. 1, pp. 66-73, Jan. 2005

[38] W.-K. D. Deslandes, "Design equations for tapered microstrip-to-Substrate Integrated Waveguide transitions," in *IEEE MTT-S Int. Microw. Symp.*, Anaheim, CA, 2010, pp. 704-707.

[39] K. Sellal, L. Talbi, T. A. Denidni and J. Lebel, "Design and implementation of a substrate integrated waveguide phase shifter," *IET Microw., Antennas & Propag.*, vol. 2, no. 2, pp. 194-199, Mar. 2008.

[40] K. Sellal, L. Talbi, T. Denidni and J. Lebel, "A New Substrate Integrated Waveguide Phase Shifter," in *European Microwave Conference*, Manchester, 2006, pp. 72-75.

[41] T. Yang, M. Ettorre and R. Sauleau, "Novel Phase Shifter Design Based on Substrate-Integrated-Waveguide Technology", *IEEE Microw. Wireless Compon. Lett.*, vol. 22, no. 10, pp. 518-520, Oct. 2012.

[42] Cong Wang, Joo Chuan Yeo, Hui Chu, Chwee Teck Lim, Yong-Xin Guo, "Design of a Reconfigurable Patch Antenna Using the Movement of Liquid Metal," *IEEE Antennas Wireless Propag. Lett.*, Vol. 17, No. 6, 2018.

[43] W. Chen, Y. Li, R. Li, A. V. Thean and Y. Guo, "Bendable and Stretchable Microfluidic Liquid Metal-Based Filter," *IEEE Microw. Wireless Compon. Lett.*, vol. 28, no. 3, pp. 203-205, Mar. 2018.

[44] C. Koo, B. E. LeBlanc, M. Kelley, H. E. Fitzgerald, G. H. Huff and A. Han, "Manipulating Liquid Metal Droplets in Microfluidic Channels With Minimized Skin Residues Toward Tunable RF Applications," *Journal Microelectr. Sys.*, vol. 24, no. 4, pp. 1069-1076, Aug. 2015.

[45] M. A. Rafi, B. D. Wiltshire and M. H. Zarifi, "Wideband Tunable Modified Split Ring Resonator Structure Using Liquid Metal and 3-D Printing," *IEEE Microw. Wireless Compon. Lett.*, vol. 30, no. 5, pp. 469-472, May 2020.

[46] A. Ha and K. Kim, "Frequency tunable liquid metal planar inverted-F antenna," *IET Elect. Lett.*, vol. 52, no. 2, pp. 100-102, Jan. 2016.

[47] A. M. Watson *et al.*, "Physically Reconfigurable RF Liquid Electronics via Laplace Barriers," *IEEE Trans. Microw. Theory Techn.*, vol. 67, no. 12, pp. 4881-4889, Dec. 2019.

[48] L. Song, W. Gao, C. O. Chui and Y. Rahmat-Samii, "Wideband Frequency Reconfigurable Patch Antenna with Switchable Slots Based on Liquid Metal and 3-D Printed Microfluidics," *IEEE Trans. Antennas Propag.*, vol. 67, no. 5, pp. 2886-2895, May 2019.

[49] T. Kim, K. Kim, S. Kim, J. Lee and W. Kim, "Micropatterning of Liquid Metal by Dewetting," *Journal Microelectr. Sys.*, vol. 26, no. 6, pp. 1244-1247, Dec. 2017.

[50] J. Low, P. Chee and E. Lim, "Deformable Liquid Metal Patch Antenna for Air Pressure Detection," *IEEE Sensors Journal*, vol. 20, no. 8, pp. 3963-3970, Apr. 2020.

[51] V. T. Bharambe, J. Ma, M. D. Dickey and J. J. Adams, "Planar, Multifunctional 3D Printed Antennas Using Liquid Metal Parasitics," *IEEE Access*, vol. 7, pp. 134245-134255, Sept. 2019.

[52] M. Wang, C. Trlica, M. R. Khan, M. D. Dickey, and J. J. Adams, "A reconfigurable liquid metal antenna driven by electrochemically controlled capillarity," *J. Appl. Phys.*, vol. 117, no. 19, May 2015.

[53] M. Wang, M. R. Khan, C. Trlica, M. D. Dickey, and J. J. Adams, "Pump free feedback control of a frequency reconfigurable liquid metal monopole," in Proc. *IEEE Int. Symp. Antennas Propag.*, 2015, pp. 2223–2224.

[54] D. Rodrigo, L. Jofre and B. A. Cetiner, "Circular Beam-Steering Reconfigurable Antenna with Liquid Metal Parasitics," *IEEE Trans. Antennas Propag.*, vol. 60, no. 4, pp. 1796-1802, Apr. 2012.

[55] S. Singh et al., "A Pattern and Polarization Reconfigurable Liquid Metal Helical Antenna," in *IEEE Int. Symp. Antennas and Propag. & USNC/URSI National Radio Science Meeting*, Boston, MA, 2018, pp. 857-858.

[56] A. Qaroot and G. Mumcu, "Microfluidically Reconfigurable Reflection Phase Shifter," *IEEE Microw. Wireless Compon. Lett.*, vol. 28, no. 8, pp. 684-686, Aug. 2018.

[57] A. Dey and G. Mumcu, "Microfluidically Controlled Frequency-Tunable Monopole Antenna for High-Power Applications," *IEEE Antennas Wireless Propag. Lett.*, vol. 15, pp. 226-229, 2016.

[58] W. Luo, H. Liu, Z. Zhang, P. Sun and X. Liu, "High-Power X-Band 5-b GaN Phase Shifter with Monolithic Integrated E/D HEMTs Control Logic," *IEEE Trans. Electron Devices*, vol. 64, no. 9, pp. 3627-3633, Sept. 2017.

[59] S. Sim, L. Jeon and J. Kim, "A Compact X-Band Bi-Directional Phased-Array T/R Chipset in 0.13 μm CMOS Technology," *IEEE Trans. Microw. Theory Techn.*, vol. 61, no. 1, pp. 562-569, Jan. 2013.

[60] S. Kagita, A. Basu and S. K. Koul, "Characterization of LTCC-Based Ferrite Tape in X-band and Its Application to Electrically Tunable Phase Shifter and Notch Filter," *IEEE Trans. Magn.*, vol. 53, no. 1, pp. 1-8, Jan. 2017.

[61] J. J. P. Venter, T. Stander and P. Ferrari, "X -Band Reflection-Type Phase Shifters Using Coupled-Line Couplers on Single-Layer RF PCB," *IEEE Microw. Wireless Compon. Lett.*, vol. 28, no. 9, pp. 807-809, Sept. 2018.

[62] F. A. Ghaffar and A. Shamim, "A Partially Magnetized Ferrite LTCC-Based SIW Phase Shifter for Phased Array Applications," *IEEE Trans. Magn.*, vol. 51, no. 6, pp. 1-8, Jun. 2015.

[63] B. Muneer, Z. Qi and X. Shanjia, "A Broadband Tunable Multilayer Substrate Integrated Waveguide Phase Shifter," *IEEE Microw. Wireless Compon. Lett.*, vol. 25, no. 4, pp. 220-222, Apr. 2015.

[64] S. I. M. Sheikh et al., "Analog/Digital Ferrite Phase Shifter for Phased Array Antennas," *IEEE Antennas Wireless Propag. Lett.*, vol. 9, pp. 319-321, Feb. 2010.

[65] Mohammad R. Khan, Chris Trlica, Michael D. Dickey, "Recapillarity: Electrochemically Controlled Capillary Withdrawal of a Liquid Metal Alloy from Microchannels," *Advanced Functional Materials*, Vol. 25, No. 5, pp. 671-678, Nov. 2014.

Shaker Alkaraki (S'17–M'19) is a post doctoral researcher at the Antennas and Electromagnetics Group at Queen Mary University of London (QMUL). Shaker received his BSc with first class Honours from IIUM Malaysia in 2011 in communication engineering, MSc with Distinction from University of Manchester (UoM) in 2013, and his PhD in electronic engineering from QMUL in 2019. He is holder of IIUM BSc scholarship, UoM MSc scholarship and QMUL PhD scholarship. His research interest includes: mm-wave and microwave reconfigurable devices, mm-wave antennas and arrays, 3D printed antennas, metallizations techniques, 5G antennas and systems, MIMO, leaky waves and reconfigurable liquid metal antennas.

Alejandro L. Borja (M'15) received the M.Sc. degree in telecommunication engineering and the Ph.D. degree from the Universidad Politecnica de Valencia, Valencia, Spain, in 2005 and 2009, respectively.

From 2005 to 2006, he was with the University of Birmingham, Birmingham, U.K. From 2007 to 2008, he was with the Universite de Lille 1, Lille, France. Since 2009, he has been with the Universidad de Castilla-La Mancha, Spain, where he is an Associate Professor.

He has published more than 70 papers in peer-reviewed international journals and conference proceedings, and frequently acts as a reviewer for several technical publications. In 2012, he served as a Lead Guest Editor for a special issue of the International Journal of Antennas and Propagation. His research interests include EM metamaterials, substrate integrate waveguide, and reconfigurable devices and their applications in microwave and millimetric bands. Dr. Borja was the recipient of the 2008 CST short paper award.

James R. Kelly (M'10) received the Master's degree in electronic and electrical engineering and the Ph.D. degree in microwave filters from Loughborough University, U.K., in 2002 and 2007, respectively.

From 2007 to 2012 he worked as a post doc. at Loughborough University, as well as the Universities of Birmingham, Durham, and Sheffield. From 2012 to 2013 he was a Lecturer at Anglia Ruskin University, Cambridge, U.K.. In 2013 he joined the Institute for Communication Systems (ICS) at the University of Surrey, U.K.. In 2018 he joined Queen Mary University of London, where he is employed as a Lecturer in Microwave Antennas.

Dr Kelly has published over 100 academic papers in peer-reviewed journals and conference proceedings. He holds a European patent on reconfigurable antennas. He is a member of the Institution of Engineering and Technology (IET), the Institute of Electrical and Electronics Engineers (IEEE). His primary research focus is reconfigurable antennas.

Raj Mittra is a Professor in the Electrical and Computer Engineering department of the Universal of Central Florida (UCF) in Orlando, FL., where he is the Director of the Electromagnetic Communication Laboratory. He also holds an appointment at the Pennsylvania State University, in University Park, PA.

Prior to joining Penn State he was a Professor in the Electrical and Computer Engineering at the University of Illinois in Urbana Champaign from 1957 through 1996.

He is a Life Fellow of the IEEE, a Past-President of AP-S, and he has served as the Editor of the Transactions of the Antennas and Propagation Society. He has received numerous

awards and medals from the IEEE, as well as from the AP Society. He was recently recognized by the URSI with the Rawer gold medal for his contributions, and was also the recipient of the Alexander Graham Bell award from the IEEE. Mittra is a Principal Scientist and President of RM Associates, a consulting company founded in 1980, which provides services to industrial and governmental organizations, both in the U.S. and abroad. A partial list of Mittra's recent publications may be found via Google Scholar Search.

Yue Gao (S'03–M'07–SM'13) is a Professor and Chair in Wireless Communications at Institute for Communication Systems, University of Surrey, United Kingdom. He received the Ph.D. degree from the Queen Mary University of London (QMUL), U.K., in 2007.

He currently leads the Antennas and Signal Processing Lab developing fundamental research into practice in the interdisciplinary area of smart antennas, signal processing, spectrum sharing, millimetre-wave and Internet of Things technologies in mobile and satellite systems.

He has published over 200 peer-reviewed journal and conference papers, 3 patents, 1 book and 5 book chapters and 3 best paper awards. He is an Engineering and Physical Sciences Research Council Fellow from 2018 to 2023. He was a co-recipient of the EU Horizon Prize Award on Collaborative Spectrum Sharing in 2016. He served as the Signal Processing for Communications Symposium Co-Chair for IEEE ICCC 2016, the Publicity Co-Chair for the IEEE GLOBECOM 2016, the Cognitive Radio Symposium Co-Chair for the IEEE GLOBECOM 2017, and the General Chair of the IEEE WoWMoM and iWEM 2017. He is the Chair of the IEEE Technical Committee on Cognitive Networks, the Secretary of the IEEE ComSoc Technical Committee Wireless Communication and the IEEE Distinguished Lecturer of the Vehicular Technology Society. He is an Editor for the IEEE Internet of Things Journal, IEEE Transactions On Vehicular Technology and IEEE Transactions on Cognitive Networks.